Journal of X-Ray Science and Technology 19 (2011) 69–90
DOI 10.3233/XST-2010-0279
IOS Press

Interior reconstruction using local inverse

Shuangren Zhao[a,*], Kang Yang[b], Dazong Jiang[c] and Xintie Yang[d]
[a]*Doubletask North York, Ontario, Canada*
[b]*University of Toronto, Toronto, Canada*
[c]*Xi'an Jiao Tong University, Xi'an, China*
[d]*Northwestern Poly Technical University Xi'an, Xi'an, China*

Received 30 June 2010
Revised 20 October 2010
Accepted 25 October 2010

Abstract. Truncated projections can arise from a detector with a limited field of view (LFOV). Truncation artifacts can be reduced through extrapolation methods; however the reconstructed images with extrapolation are often over-corrected or under-corrected. Recently, an iterative reconstruction-reprojection algorithm was developed, which incorporated extrapolation with iterative algorithm. It gave the possibility to better reduce truncation artifacts compared to using the extrapolation method alone. This article builds a theoretic foundation for the above iterative reconstruction-reprojection algorithm. The theoretic foundation is suitable to parallel-beam, fan-beam and cone-beam computed tomography(CT). Two assumptions are summarized from the CT system. Then, a truncation-artifact-free solution for the problem of LFOV is derived from these assumptions. The solution contains a "local inverse" of matrix. The local inverse of a matrix is defined using the sub-matrix and its general inverse. The solution can be approximately implemented as the iterative reconstruction-reprojection algorithm which is just the algorithm mentioned above.

Keywords: Artifact, truncation, image, reconstruction, projection, extrapolation, LFOV, tomography, local, inverse, CT, SPECT, PET

1. Introduction

The width of our cone-beam CT(computed tomography) detector is about 40 cm, and the field of view (FOV) of the detector is around 26 cm; dependent on the magnification of the CT system. If parts of an object to be reconstructed are out of the FOV of the detectors, the measured projections are truncated. Figure 1 shows the gemetries of CT or SPECT(Single Photon Emission Computed Tomography) systems which can be parallel-beam, fan-beam, or cone-beam gemetries. Here, fan-beam geometric is shown as an example.

Filtered backprojection(FBP) method [1] is often utilized to reconstruct images from parallel-beam and fan-beam tomographic projections. For cone-beam reconstruction there are methods [2,3]. A recent publication in cone-beam reconstruction with nor-circular geometry can be seen in reference [4].

The reconstruction with truncated projections using FBP method produces truncation artifacts, which are bright rings on the boundary of the region of interest (ROI). This reconstruction is one of the problems

*Corresponding author: Shuangren Zhao, 113 Mintwood Dr., North York, Ontario M2M 3A6, Canada. E-mail: shrzhao@rogers.com.

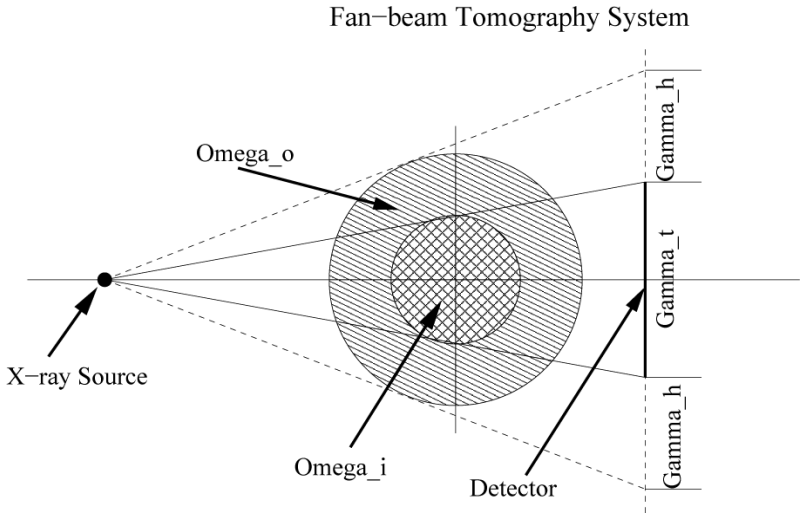

Fig. 1. CT and SPECT geometries are shown as an example. In the figure Ω_i is written as Omega_i for example, because of lack of fonts. Here Ω_i is the interior of ROI, Ω_o is the outside of ROI. Γ_t is the region for truncated projection. Γ_h is the region to define hollow projections.

of LFOV. The ROI is an area in which the reconstruction is to be made. It is assumed in this article that the ROI is corresponding to the FOV of the detector i.e. the diameter of the ROI is equal to the FOV of the detector, resulting in the absence of a margin between the ROI and FOV (see Fig. 1).

The truncation artifacts can be reduced through extrapolation of the missing rays [5,6]. The reconstructed images are strongly influenced by different extrapolation methods, for example, constant, linear, or exponential extrapolations. The reconstructed images are often over-corrected or under-corrected through different extrapolations. If the image is over-corrected, the bright rings change to dark rings. If the image is under-corrected, the bright rings become weak but still remain visible. Improved results are available from iterative extrapolation [12–14] and adaptive extrapolation [16–18].

The wavelet method [5,7] usually utilises the extrapolation process. The reference [5] has found that it is not the wavelets that are important to reduce the truncation artifacts, but rather an extrapolation of the local data. Utilizing the priori for the LFOV problem was studied by reference [8]. If the part of an object that lies outside of the ROI does not surround the ROI, Hilbert transform method [9] can offer an exact solution for the problem of LFOV. An improved Hibert transform method can be found [19,22]. A Generalized method corresponding to Hibert transform method for cone-beam situation can be found in [20].

There are exact interior reconstruction methods [19,22]. This kind of interior algorithm is exact on the sense that there is at least one pixel of the image inside the interior region is known before reconstruction. The implementation of the algorithm is a iterative algorithm: the projection onto convex sets (POCS) method, which has the calculation errors. Since this error, the truncation artifacts are visiable even on the figures of the articles [19,22]. Reference [21] is trying to improve the POCS method and reduce its error.

Local tomography [10,11] is also often utilized to treat the truncation artifacts. The truncation artifacts can be eliminated with local tomography. Hence it is a truncation-artifact-free algorithm. Artifacts are signal related. Truncation artifact is related to the object outside the ROI. Interior cupping artifact is related only with object inside the ROI. Local tomograpy is more sensitive to noise than the FBP method and it introduces another kind of artifact i.e. interior cupping artifacts.

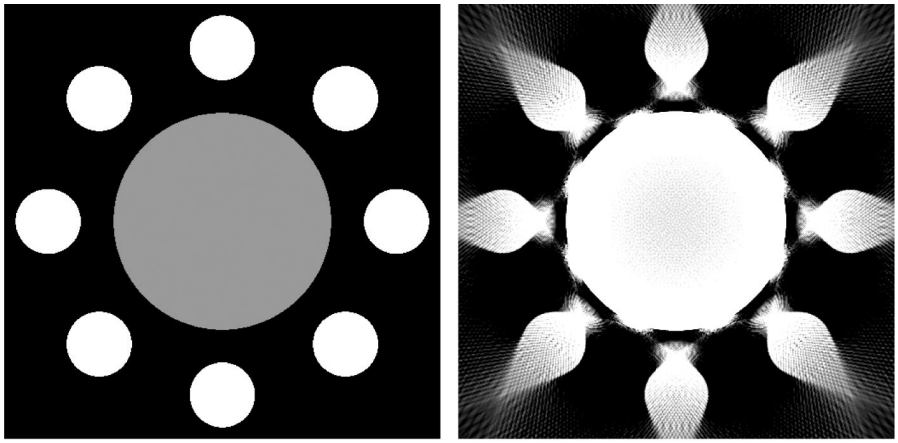

(a) (b)

Fig. 2. (a) Is a phantom with 8 small disks outside ROI and a big disk just inside ROI. (b) Is the reconstruction of the phantom (a) Using FBP method without extrapolation. The projections are truncated and the FOV is just half the width of the image.

An iterative reconstruction-reprojection algorithm [15] was designed for the problem of LFOV. Figure 2 is used to explain this algorithm. Figure 2a shows the phantom and Fig. 2b shows the rough reconstruction using FBP method in the case of LFOV. The phantom consists of 8 small disks outside its ROI and a big disk just inside its ROI. Figure 2b indicates that the big disk was reconstructed with strong truncation artifacts and the 8 small disks were reconstructed roughly. The image size was 512×512. The simulated projections were produced from parallel-beam geometries. The number of projections for a half circle (180°) scan was 360. The space between two elements of the detector was assumed to be the same as the distance between two pixels of the image. The motive of the algorithm [15] was to correct the truncated projections through the reconstructed image outside the ROI, which is the blurred image of 8 small disks (See Fig. 2b). The correction is done by added the projection data of the negative values of the blurred image the of 8 small disks. It was thought that the corrected projections plus extrapolation could yield better reconstruction results than using extrapolation alone.

This article studies the theoretic foundation of the problem of LFOV. The characters of parallel-beam, fan-beam and cone-beam CT are summarized as two assumptions. The assumptions are approximately satisfied by the numerical methods for example FBP method. It is assumed that there exists an abstract reconstruction algorithm which satisfies these assumptions. Two algorithms are deduced from these assumptions of the LFOV problem.

One of them is the solution of local inverse. Local inverse is an inverse algorithm which eliminates the influences from the outside the ROI. The error analysis is done for these algorithms using the assumptions. The error analysis deduces that the algorithm with the local inverse is a truncation-artifact-free solution. Here, truncation artifacts free does not mean that the artifacts are free. Another kind of artifact that still exists that is the interior cupping artifact. This is similar to local tomography. The iterative reconstruction-reprojection algorithm [15] can be seen as an implementation of the local-inverse algorithm. The local-inverse algorithm has the interior cupping artifact, but it is usually weaker than that of local tomography. The extrapolations used in the implementation of the local inverse can furthermore reduce the interior cupping artifact. The interior cupping artifacts of local inverse can normally been seen in reconstructed image clearly. However the example of this article shows the cupping artifact of local inverse with two extrapolations are not visible in the reconstructed image.

An example about the local inverse of a matrix instead of image reconstruction is given to show that the idea of local inverse is not restrict to image reconstruction. It is a important concept to reduce the influence from out side of ROI.

2. The problem of LFOV

Assume that $X = X(x)$ is the original image. x is the pixel of the image and $p = (\theta, u)$ are parallel beam projections. (θ, u) is the angle and position of the detector channel. Also assume that Ω_i is the inside of the ROI and Ω_o is the outside of the ROI. X_i expresses the part of the object on Ω_i. X_o expresses the part of the object on Ω_o. Γ_t is the region inside the FOV of the detector. Γ_h is the region outside the FOV of the detector. p_t expresses the truncated projections on Γ_t. p_h expresses the hollow projections on Γ_h. The sketch of CT system can be seen in Fig. 1. The mathematical model of CT system can be expressed as following,

$$\begin{bmatrix} p_t \\ p_h \end{bmatrix} = \begin{bmatrix} P_{ti} & P_{to} \\ P_{hi} & P_{ho} \end{bmatrix} \begin{bmatrix} X_i \\ X_o \end{bmatrix} \tag{1}$$

Here $p = [p_t, p_h]^T$ expresses projections. Superscript T indicates the transpose matrix. $X = [X_i, X_o]^T$ expresses the object or original image. P and X are operator. $P = \begin{bmatrix} P_{ti} & P_{to} \\ P_{hi} & P_{ho} \end{bmatrix}$ is a known projection operator which can be Radon transform for example. In this article an operator and its corresponding matrix are treated as the same. P_{ti}, P_{to}, P_{hi} and P_{ho} are sub-matrixes of the projection operator P. The subscript expresses the definition region and the transformation region of the operator. For example P_{ti} is the projection operator from Ω_i to Γ_t. Assume that there exists a reconstruction operator $R = \begin{bmatrix} R_{it} & R_{ih} \\ R_{ot} & R_{oh} \end{bmatrix}$ in full field of view(FFOV) and the image can be reconstructed from projections p,

$$\begin{bmatrix} X_i^r \\ X_o^r \end{bmatrix} = \begin{bmatrix} R_{it} & R_{ih} \\ R_{ot} & R_{oh} \end{bmatrix} \begin{bmatrix} p_t \\ p_h \end{bmatrix} \tag{2}$$

Here, $X^r = [X_i^r, X_o^r]^T$is a reconstructed image of $X = [X_i, X_o]^T$. R_{it}, R_{ih}, R_{ot} and R_{oh} are the sub-matrixes of the reconstruction operator R. The subscripts of the sub-operator express the definition region and the transformation region of the operator. For example R_{it} expresses the reconstruction operator from Γ_t to Ω_i.

Assume that the sub-matrixes P_{ti}, P_{to}, P_{hi}, P_{ho} and R_{it}, R_{ih}, R_{ot}, R_{oh} are all known. Also assume that the truncated projections p_t are known but the hollow projections p_h are unknown. Finally, assume that the object X_i, X_o are unknown. The problem here is how to solve the part of the object X_i. The part of the object X_o is not required to be found. The first row of Eq. (1) can be written as

$$p_t = P_{ti}X_i + P_{to}X_o \tag{3}$$

if X_i directly reconstructed from Eq. (3), there is

$$\hat{X}_i = R_{it}\, p_t = R_{it}(P_{ti}X_i) + R_{it}P_{to}X_o \tag{4}$$

$\hat{X}_i$ is the reconstructed image. The first item is the reconstructed image if the field of view of the detector is not limited. The last item of right side of Eq. (4) $R_{it}P_{to}X_o$ represents truncation artifacts which relate

part of object on Ω_o. In this case the reconstructed image suffers severe truncation artifacts. This is the problem of LFOV. This article looks for the algorithms which can better reduce the truncation artifacts. Here the concrete form of the sub-matrices P_{ti}, P_{to}, P_{hi}, P_{ho} and R_{it}, R_{ih}, R_{ot}, R_{oh} are not given. Instead, the characteristics of these sub-matrixes are summarized.

3. Characteristics of the tomography systems

The characteristics of the CT systems are summarized as 2 assumptions in the following.

Assumption I. Assume that a reconstruction algorithm R exists with which the reconstructed image is equal to the original image, i.e.,

$$X^r = X \tag{5}$$

X^r is defined in Eq. (2). The above Eq. (5) means

$$R\,P\,X = X \tag{6}$$

This assumption requires that R is an exact reconstruction operator. Strictly speaking, the reconstruction operator, for example, FBP method is not an exact reconstruction operator. Usually the reconstructed image using FBP method will become obtuse near the image edges. However the FBP method is a very good approximation of an exact reconstruction operator. Equation (6) can be satisfied in the limit if the number of channels for the CT detector increases to infinity.

In this assumption, R is an abstract reconstruction operator which represents many practical reconstruction algorithms including FBP method.

Assumption II. Suppose that the object X_i on sub-region Ω_i is a region without hole inside, then there is no contribution to the projection in the region Γ_h, i.e.,

$$P_{hi}X_i = 0 \tag{7}$$

Here Γ_h is the outside of the region Γ_t and Γ_t is the FOV corresponding to the region Ω_i.

This assumption requires that the part of the object on the region Ω_i does not contribute to the hollow projections on the region Γ_h. This characteristic is satisfied by all CT systems as long as X-ray goes along a line and the scattering effect of an X-ray can be omitted.

Corollary 1. Assume that Ω_i is an arbitrary sub-region which has no hole inside. $P_{ti}X_i$ are the projections produced from the object on Ω_i. If a reconstruction is made from the part of projections, then there is

$$R_{it}P_{ti}X_i = X_i \tag{8}$$

Corollary 2. If a reconstruction is made from the part of projections same as corollary 1, then it has no contribution to the region Ω_o, i.e,

$$R_{ot}P_{ti}X_i = 0 \tag{9}$$

These two corollaries are clear in intuition. However proof is available in the following which utilized the above two assumptions only.

Proof for Corollary 1 and Corollary 2. Considering X_i is a special case of X in which the object satisfies $X_o = 0$, i.e.

$$X = [X_i, 0]^T \tag{10}$$

In this case the first row of Eq.(1) can be written as

$$p_t = P_{ti} X_i \tag{11}$$

The second row of Eq. (1) can be written as

$$p_h = P_{hi} X_i \tag{12}$$

Considering assumption II

$$p_h = 0 \tag{13}$$

Considering Eq. (13), Eq. (2) can be written as

$$\begin{bmatrix} X_i^r \\ X_o^r \end{bmatrix} = \begin{bmatrix} R_{it} p_t \\ R_{ot} p_t \end{bmatrix} \tag{14}$$

Considering assumption I and Eq. (10) in the left of the above equation and substituting Eq. (11) in the right of the above equation we get

$$\begin{bmatrix} X_i \\ 0 \end{bmatrix} = \begin{bmatrix} R_{it} P_{ti} X_i \\ R_{ot} P_{ti} X_i \end{bmatrix} \tag{15}$$

The first row of above equation is corollary 1 and the second row of above equation is corollary 2.

Corollary 3. If X_o is known, the contribution of X_o to the projections on the region Γ_t can be calculated. This contribution is $P_{to} X_o$. It can be taken away from the projections. The projections $p_t - P_{to} X_o$ will not contain the contribution from original image on the region Ω_o. Using these projections the part of image on the region Ω_i can be obtained, which is

$$X_i = R_{it}(p_t - P_{to} X_o) \tag{16}$$

This corollary is also clear in intuition. The proof for this corollary using the first corollary can be found in the following.

Proof for Corollary 3. The Eq. (3) can be rewritten as

$$P_{ti} X_i = p_t - P_{to} X_o \tag{17}$$

By substituting Eq. (17) to Corollary 1 (Eq. (8)), we get Eq. (16).

4. Two reconstruction algorithms for LFOV

Equation (16) tells us that if X_o is known then X_i can be obtained. Simulations tell us that finding an exact X_o is not necessary. In order to get an accurate reconstruction of X_i, all that is necessary is to find a $\hat{X}_o$ that is roughly close to X_o. According to this idea two algorithms are derived in the following.

4.1. The first algorithm

The second row of Eq. (2) and assumption I yields

$$X_o = R_{ot}p_t + R_{oh}p_h \tag{18}$$

Since p_h is unknown, the second item of the above equation can not be calculated. Taking p_h as zero, an approximation of X_o is obtained

$$\hat{X}_o = R_{ot}p_t \tag{19}$$

Substituting $\hat{X}_o$ in the above Eq. (19) to the variable X_o in Eq. (16), an approximation of X_i is obtained

$$\hat{X}_i^A = R_{it}(I - P_{to}R_{ot})\,p_t \tag{20}$$

Where $\hat{X}_i^A$ is the approximation of X_i. Superscript ^{A} expresses the first algorithm. I is identical operator or unit matrix.

4.2. The second algorithm

Create a matrix G from P_{to} similar to Eq. (66) in Appendix

$$G = [I - P_{to}P_{to}^{+}] \tag{21}$$

Considering Eqs (21) and (70) in Appendix, it follows that G is perpendicular to P_{to} i.e.,

$$G\,P_{to} = 0 \tag{22}$$

The Eq. (3) can be written as

$$p_t = p_{ti} + p_{to} \tag{23}$$

Where $p_{ti} = P_{ti}X_i$ represents the part of truncated projections contributed by X_i and $p_{to} = P_{to}X_o$ represents the part of truncated projections contributed by X_o. Considering Eq. (23), Eq. (22) and $p_{to} = P_{to}X_o$, we get

$$G\,p_t = G\,p_{ti} \tag{24}$$

The above equation means that the operator G can filter out the projection variable p_{to}. p_{ti} can be solved using general inverse

$$\hat{p}_{ti} = G^{+}G\,p_t \tag{25}$$

Considering Eqs (69 and 67) in Appendix, the Eq. (25) can be rewritten as

$$\hat{p}_{ti} = G\,p_t \tag{26}$$

Eq.(8) can be written as

$$X_i = R_{it}\,p_{ti} \tag{27}$$

Substituting $\hat{p}_{ti}$ to the variable p_{ti} in Eq. (27) and considering Eq. (21), the solution for X_i is obtained,

$$\hat{X}_i^B = R_{it}(I - P_{to}P_{to}^+)\, p_t \tag{28}$$

$\hat{X}_i^B$ is the solution of $\hat{X}_i$ with this second algorithm.

The two algorithms are similar. They can be summarized as two-step algorithms. The first step is to calculate $\hat{p}_{to}$. Corresponding to the two algorithms, $\hat{p}_{to}$ is represented by $\hat{p}_{to}^A = P_{to}R_{ot}\, p_t$, $\hat{p}_{to}^B = P_{to}P_{to}^+\, p_t$ respectively. The second step is to calculate $\hat{X}_i$ by $\hat{X}_i = R_{it}(p_t - \hat{p}_{to})$.

The first algorithm Eq. (20) is practical in real calculation, because it only consists of matrix multiplication. The second algorithm Eq. (28) is difficult in numerical calculation because it consists of general inverse of matrix. However the second algorithm Eq. (28) has more theoretical values.

5. Local inverse

The above discussion can be summarized as local inverse. Local inverse can be used to a kind inverse problem where part of the measured data is unknown.

5.1. Definition of local inverse

Define a local inverse $P_{ti}^{\sim}$ of the matrix P (Eq. (1)) on the region Γ_t to the region Ω_i as following,

$$P_{ti}^{\sim} = P_{ti}^+(I - P_{to}P_{to}^+) \tag{29}$$

If the normal matrix inverse P_{ti}^{-1} existed, P_{ti}^+ can be replaced by P_{ti}^{-1}. P_{ti}^{-1} is a better inverse compared to P_{ti}^+ and P_{ti}^{-1} also belongs to general inverse P_{ti}^+.

In the case of X-ray tomography considering Eq. (8), there is

$$P_{ti}\, R_{it}\, P_{ti}X_i = P_{ti}\, X_i \tag{30}$$

or

$$P_{ti}R_{it}P_{ti} = P_{ti} \tag{31}$$

Hence R_{it} is the a general inverse of P_{ti}. P_{ti}^+ can be replaced as R_{it}. Hence this algorithm Eq. (28) can be seen as the solution with the local inverse.

5.2. A example of local inverse

In order to understand the idea of local inverse, a example with a simple matrix is given in the following.

This example is not in the case of X-ray tomography. It is a problem of reconstructing 1-dimensional image from a part of its matrix transformation.

Assume that the original image is $X = [X_i, X_o]^T$ which is defined as

$$X_i = \begin{bmatrix} 0 \\ 0.8660 \\ 0.8660 \\ 0 \\ -0.8660 \\ -0.8660 \\ 0 \end{bmatrix} \quad X_o = \begin{bmatrix} 1 \\ 1 \\ 1 \\ 1 \end{bmatrix} \tag{32}$$

A transformation of image is defined as $p = P\,X$. Here P is a known matrix transform $P = \begin{bmatrix} P_{ti} & P_{to} \\ P_{hi} & P_{ho} \end{bmatrix}$ which is defined as

$$P_{ti} = \begin{bmatrix} 5\,5\,5\,3\,5\,5\,5 \\ 5\,5\,1\,1\,5\,1\,3 \\ 3\,1\,5\,3\,1\,1\,3 \\ 1\,5\,3\,1\,1\,1\,1 \\ 1\,3\,1\,3\,5\,1\,1 \\ 1\,3\,3\,3\,1\,3\,3 \\ 1\,3\,3\,5\,5\,3\,1 \end{bmatrix} \; P_{to} = \begin{bmatrix} 4\,4\,4\,1 \\ 1\,1\,3\,1 \\ 3\,4\,4\,1 \\ 4\,4\,3\,4 \\ 3\,1\,4\,3 \\ 4\,1\,1\,3 \\ 4\,4\,3\,4 \end{bmatrix} \tag{33}$$

$$P_{hi} = \begin{bmatrix} 0\,0\,0\,0\,0\,0\,0 \\ 0\,0\,0\,0\,0\,0\,0 \end{bmatrix} \; P_{ho} = \begin{bmatrix} 1\,3\,1\,1 \\ 1\,9\,9\,3 \end{bmatrix}$$

It is noted that $P_{hi} = 0$, which is similar to the X-ray tomography situation Eq. (7). Instead knowing the whole transformation $p = P\,X$, a part of the transformation of the image

$$p_t = P_{ti}X_i + P_{to}X_o \tag{34}$$

is measured (or simulated), which is given in the following:

$$p_t = \begin{bmatrix} 13.000 \\ 6.000 \\ 15.4641 \\ 20.1962 \\ 9.2679 \\ 10.7321 \\ 11.5359 \end{bmatrix} \tag{35}$$

Assume that the two parts of the image X_i and X_o are unknown. The problem is to reconstruct the image X_i from the part of the transformation of the image p_t (Eq. (35)). Here X_o does not need to be recovered and $P = \begin{bmatrix} P_{ti} & P_{to} \\ P_{hi} & P_{ho} \end{bmatrix}$ is known by Eq. (33). If the image can be reconstructed using general inverse, the result is

$$\hat{X}_i = P_{ti}^{+}\,p_t = \begin{bmatrix} -0.2045 \\ 2.4569 \\ 3.6009 \\ 1.4167 \\ -0.4115 \\ -1.4266 \\ -2.2652 \end{bmatrix} \tag{36}$$

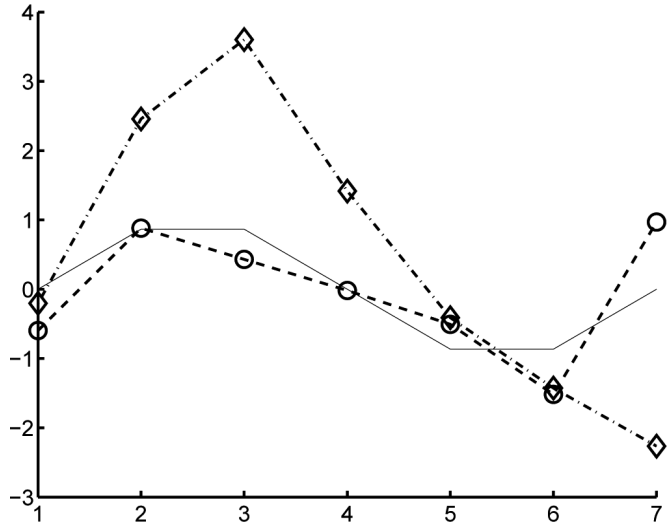

Fig. 3. 1-dimensional image reconstruction with local inverse and general inverse. The solid line is the original image. The dashed line with circle is the reconstruction with local inverse. The dash-dot line with diamond is the reconstruction with general inverse.

If the image is reconstructed using local inverse Eq. (29)

$$\hat{X}_i = P_{ti}^{\sim}\, p_t = P_{ti}^{+}[I - P_{to}P_{to}^{+}]\, p_t = \begin{bmatrix} -0.5971 \\ 0.8812 \\ 0.4312 \\ -0.0181 \\ -0.5068 \\ -1.5181 \\ 0.9686 \end{bmatrix} \tag{37}$$

Figure 3 shows that the image reconstructed with local inverse is quite close to the original image. The image reconstructed with general inverse has a larger error compared to the error of the image reconstruction using the local inverse. The following analysis will discuss the errors of these algorithms.

6. Error analysis

Define the error as

$$X_{id}^{m} = \hat{X}_i^m - X_i \tag{38}$$

where $m = A, B$ which is corresponding to the first algorithm Eq. (20) and the second algorithm Eq. (28) respectively.

6.1. The error of the second algorithm

By multiplying the matrix P_{to}^{+} to the two sides of Eq. (3) we get

$$P_{to}^{+}p_t = P_{to}^{+}(P_{ti}X_i + P_{to}X_o) \tag{39}$$

By substituting the above equation to Eq. (28), we get

$$\hat{X}_i^B = R_{it}(p_t - P_{to}P_{to}^+P_{ti}X_i - P_{to}P_{to}^+P_{to}X_o) \tag{40}$$

By substituting Eqs (40) and (16) to Eq. (38) we get

$$X_{id}^B = -R_{it}(P_{to}P_{to}^+P_{to} - P_{to})X_o - R_{it}P_{to}P_{to}^+P_{ti}X_i \tag{41}$$

Considering Eq. (65) in Appendix, we get

$$X_{id}^B = -R_{it}P_{to}P_{to}^+P_{ti}X_i \tag{42}$$

This is the error of the algorithm Eq. (28). It is known that truncation artifacts are errors caused by an unknown object outside ROI, i.e. X_o. This error Eq. (42) is not related to X_o and it is only related to X_i, which means that this algorithm is truncation artifacts free. By the way, the local tomography [10] is also a truncation-artifact-free algorithm and the reconstructed image with local tomography is cupped. Hence the local inverse algorithm Eq. (28) is similar to the local tomography. The right side of Eq. (42) gives the interior cupping artifacts of the algorithm of Eq. (28). The authors hope that the interior cupping artifacts with this algorithm Eq. (28) is smaller than the local tomography.

The necessary condition for local inverse to work well requires that the error (Eq. (42)) is small. This condition can be given in quantity,

$$\frac{||P_{ti}^+P_{to}P_{to}^+P_{ti}X_i||}{||X_i||} \ll 1 \tag{43}$$

$||\bullet||$ is a L1 (or L2) mode of a vector. The left side of Eq. (43) can be seen as the crosstalk from operator P_{ti} to P_{to}. Hence the necessary condition of the local inverse works well is that the crosstalk is much smaller than 1.

In the section 5, the result of local inverse is better than the result of general inverse. The problem of the general inverse algorithm is the truncation artifacts since p_h is unknown and p_h is set to 0. The local inverse algorithm replaces the truncation artifacts to the interior cupping artifacts. As long as the interior cupping artifact is weaker than the truncation artifact, the local inverse can obtain better result compared to the general inverse algorithm.

6.2. The error of the first algorithm

Similar to Eq. (41) the error corresponding the first algorithm is

$$X_{id}^A = -R_{it}(P_{to}R_{ot}P_{to} - P_{to})X_o - R_{it}P_{to}R_{ot}P_{ti}X_i \tag{44}$$

Considering Eq. (9), The above equation yields

$$X_{id}^A = -R_{it}(P_{to}R_{ot}P_{to} - P_{to})X_o \tag{45}$$

From the above error analysis, it is clear that these two algorithms all have the advantages and disadvantages. The advantage of the first algorithm is that X_{id}^A is independent to X_i, hence it has no interior cupping artifact. The disadvantage of the first algorithm is that the truncation artifact is not 0 Eq. (45). The advantage of the second algorithm is that X_{id}^B is independent to X_o, hence it is truncation-artifact-free. The disadvantage of the second algorithm is that the reconstructed image is with interior cupping artifact Eq. (42).

7. Implementation of local inverse algorithm

Equation (28) can be written as the following two-step algorithm,

$$\hat{X}_o = P_{to}^{+}\, p_t \tag{46}$$

$$\hat{X}_i = R_{it}(p_t - P_{to}\hat{X}_o) \tag{47}$$

In the above equation $\hat{X}_i^B$ is written as $\hat{X}_i$ for simplification. Equation (46) can be implemented through solving the linear equation,

$$P_{to}X_o = p_t \tag{48}$$

Considering P_{to}^{-} as an approximation inverse operator of P_{to}, the above linear equation can be solved iteratively with P_{to}^{-}

$$p_t^{(0)} = p_t \tag{49}$$

$$p_t^{(n)} = p_t - P_{to}\hat{X}_o^{(n-1)} \tag{50}$$

where $\hat{X}_o^{(n-1)}$ $n = 0, 1, 2\cdots$ is obtained in the following,

$$Y_o^{(n)} = P_{to}^{-}\, p_t^{(n)} \tag{51}$$

$$\hat{X}_o^{(n)} = \sum_{i=0}^{n} Y_o^{(i)} \tag{52}$$

$\hat{X}_o^{(n)}$ in Eqs (49–52) gives an implementation of $\hat{X}_o$ in Eq. (46). The whole algorithm Eqs (46, 47) is done by combining Eqs (49–52) together with Eq. (47). This iterative algorithm can be further simplified as

$$p_t^{(0)} = p_t \tag{53}$$

$$p_t^{(n)} = p_t^{(n-1)} - P_{to}\, P_{to}^{-}\, p_t^{(n-1)} \tag{54}$$

$$\hat{X}_i = R_{it}\, p_t^{(n)} \tag{55}$$

About P_{to}^{-}, there are two choices; $P_{to}^{-} = P_{to}^{T}$ and $P_{to}^{-} = R_{ot}$. Here ^{T} expresses the matrix transposition. P_{to}^{T} is a backprojection operator. R_{ot} is a filtered backprojection operator $R_{ot} = P_{to}^{T}\, F$, here F is a filtering operator. The first choice is to find a solution $\hat{X}_o$ for Eq. (46), since P_{to}^{T} has the exact same number of singular values and same singular value decomposition matrixes U, V with P_{to} and P_{to}^{+}. The second choice is to find a solution $\hat{X}_o$ for Eq. (48) and disregard whether it is close to P_{to}^{+} or not. Section 4 has mentioned that the solution of $\hat{X}_o$ is not necessary to be very accurate. Hence both solutions should be good. The key is which one has a better performance in implementation.

The algorithm Eqs (53,54 and 55) was obtained from Eq. (20) by directly adding more loops of iteration without mentioning the reason why more loops are suitable [15].

In the practical implementation, the reconstruction algorithm (R) for FFOV is usually not an exact inverse operator. The implementation of Eqs (49–52) is also not an exact equivalent to the algorithm Eq. (46). Thus Eqs (53, 54 and 55) are not exactly equivalent to the algorithm Eq. (28). It is proved that Eq. (28) has also interior cupping artifact. Simulation results showed that the effect of the truncation artifact reduction using the iterative algorithm Eqs (53–55) is not ideal. The results are not presented here because of the length limitation of this article. In order to overcome this difficulty extrapolation is utilized as additional help to the algorithm. Considering the extrapolation and adjusting the operator the algorithm Eqs (53–55) can be rewritten as the following,

$$p^{(0)} = E\, p_t \tag{56}$$

$$p^{(n)} = E\,(p^{(n-1)} - P\,\omega_o\, R\, p^{(n-1)}) \tag{57}$$

$$\hat{X} = R\, p^{(n)} \tag{58}$$

$\hat{X}_i$ can be obtained from equation $\hat{X}_i = \omega_i \hat{X}$. R in the above equation can be FBP algorithm. Here E is the extrapolation operator. Many different extrapolations can be applied, for example constant extrapolation, quadratic extrapolation, exponential extrapolation and so on. ω_i and ω_o are operators which are defined as

$$\omega_i = \begin{cases} 1\, if & x \in \Omega_i \\ 0\, if & x \notin \Omega_i \end{cases} \tag{59}$$

$$\omega_o = \begin{cases} 1\, if & x \in \Omega_o \\ 0\, if & x \notin \Omega_o \end{cases} \tag{60}$$

In the derivation of Eqs (57 and 58) the first choice is taken, i.e. $P_{to}^{-} = R_{ot}$ since it has a better performance after cooperating with extrapolation. The following relationships have been considered $R_{ot} \rightarrow \omega_o\, R\, E$, $P_{to} \rightarrow E\, P\, \omega_o$, $R_{it} \rightarrow \omega_i R E$. The above Eqs (56–58) are the iterative algorithm of reference [15].

The above work is the implementation of the second algorithm Eq. (28). The implementation of the first algorithm Eq. (20) is same as Eqs (56–58) unless the iteration number is 1 (2 reconstructions) instead of n. Hence the first algorithm can be seen as a special approximation of the the second algorithm.

8. Example of the iterative algorithm with extrapolation

In order to compare the reconstructed image with original phantom, similar to the reference [14] the distance d from the reconstructed image g to original image f is defined as following:

$$d = \frac{\sum_{i=1}^{N} \sum_{j=1}^{N} |\Omega_i\,(g_{ij} - f_{ij})|^2}{\sum_{i=1}^{N} \sum_{j=1}^{N} |\Omega_i\,(f_{ij} - \bar{f})|^2} \tag{61}$$

where N is the size of elements of the image. In the following we always calculate the distances from the reconstructed images to the phantom. It is remarkable that for distance calculation, only the part of image inside the ROI is taken into consideration and hence here the truncation operator Ω_i is utilized. $\bar{f}$ is average of the image f defined as $\bar{f} = \frac{1}{N^2} \sum_i^N \sum_j^N \Omega_i\, f_{ij}$.

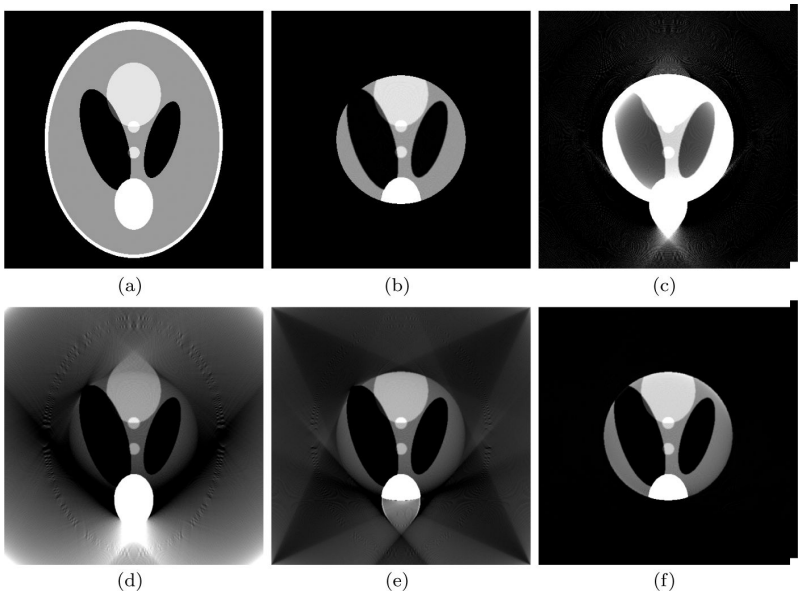

Fig. 4. Reconstruction with truncated projections. (a) The phantom of a body with arm on the bourder of ROI. (b) The ideal reconstruction using FBP method, the image is croped. (c) The reconstruction without extrapolation. (d) The reconstruction with constant extrapolation. (e) The 2ed reconstruction in the iteration. (f) The 20th reconstruction in the iteration.

8.1. The first example

Phantom is slightly modified Shepp-Logan head phantom. This phantom is simulated the situation of a human body with its arm on the border of the ROI.

The data size of the phantom and the reconstruction is 512×512. The image width and height are 1 unit-length. The space between two channels of detector is assumed to be the same as the distance between two pixels of the image. The number of projections is 360 for a half circle (180°) scan. We choose the radio of the crop is $a = 0.5$ unit-length. The extrapolation is using constant extrapolation see the following formula [15],

$$(E\,p)(\theta,u) = \begin{cases} p(\theta,-a) & \text{if } u < -a \\ p(\theta,u) & \text{if } |u| \leqslant a \\ p(\theta,a) & \text{if } u > a \end{cases} \tag{62}$$

Figure 4 shows the reconstructions for different iteration number. Figure 5 shows the distances of the reconstructions versus the number of iteration. The smallest distance is $d = 0.0356$ and it is achieved at 47-th reconstruction of iteration. The ideal distance for this situation is calculated $d = 0.0129$. Hence the smallest distance of this iterative algorithm is not too far away from the ideal distance.

8.2. The second example

In first example the constant extrapolation is utilized. The iteration begin diverges from 47-th reconstruction of iteration. In the second example we consider the situation that the massive object is at outside of the ROI. We have found in this case if constant extrapolation is used, the algorithm begins diverge only after a few reconstructions of the iteration. The truncation artifact is reduced but still visible. in order further improve the algorithm, more sophistical extrapolation is utilized here.

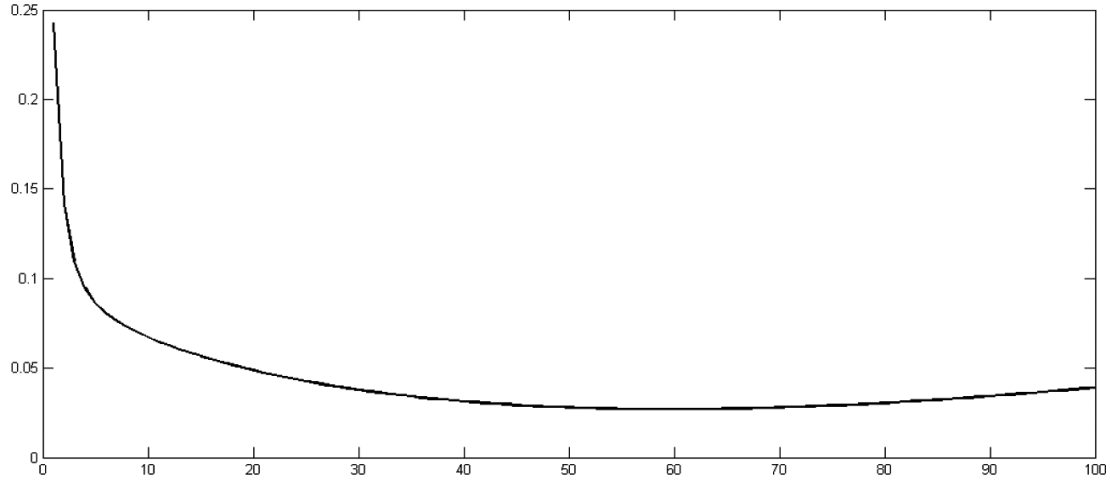

Fig. 5. The distances of the iterative reconstruction for modified Shepp-Logan head phantom versus the number of iteration.

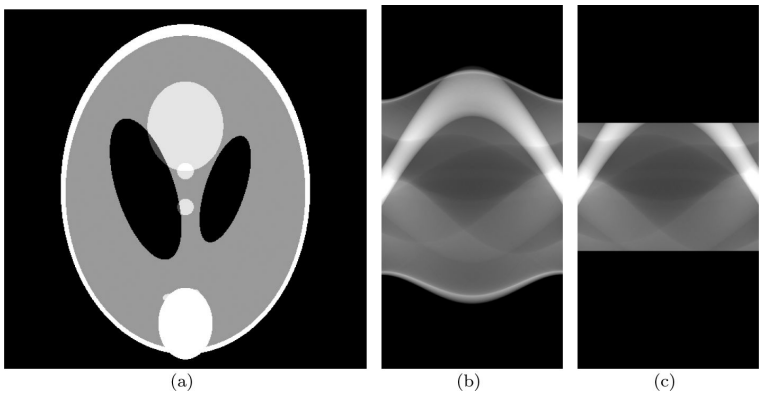

Fig. 6. (a) Phantom. (b) Projections in case of FFOV. (c) Truncated projections in case of LFOV.

Figure 6a shows the strongly modified Shepp Logan Phantom. A massive object (i.e. a small bright ellipse disk) is added to the Shepp Logan phantom in the region Ω_o. A massive object in Ω_o is added to increase the difficulty of the reconstruction in the problem of LFOV . Simulations showed that many extrapolation algorithms can obtain good results for reduction of the truncation artifacts if the Shepp Logan phantom or the phantom in 4(a) where the massive object was on the border of ROI was used but they did not succeed with the strongly modified Shepp Logan phantom in Fig. 6(a). Figure 6(b) shows the untruncated projections which are obtained by simulation with parallel-beam geometries using Radon transform. Figure 6(c) shows the truncated projections which is obtained by setting zeros in the region Γ_h of the untruncated projections. In this example, the width of the FOV is just half the length of the image. The data size of the phantom and the reconstruction is 512×512. The space between two channels of detector is assumed to be the same as the distance between two pixels of the image. The number of projections is 180 for a half circle (180°) scan.

Figure 7a shows the reconstruction from truncated projections using FBP method with extrapolation. The extrapolation operator E is a mixture combining quadratic extrapolation and exponential

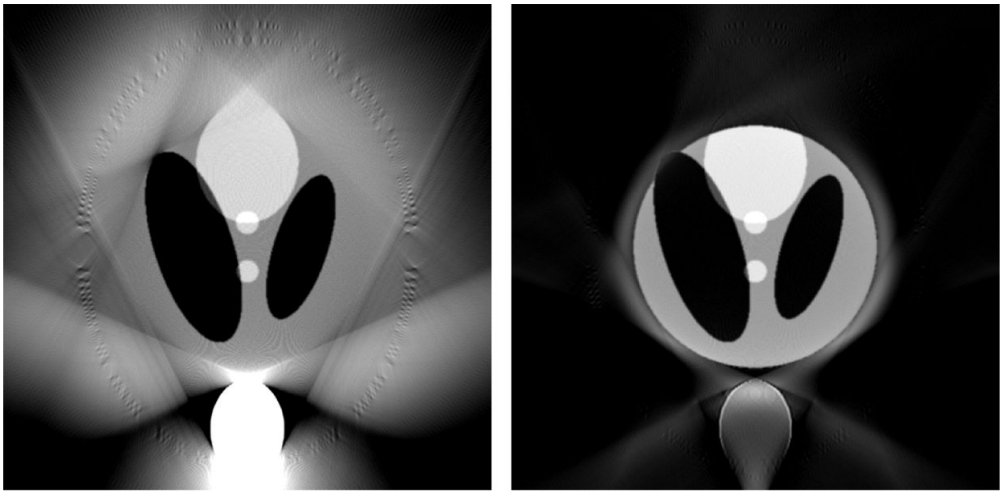

(a) (b)

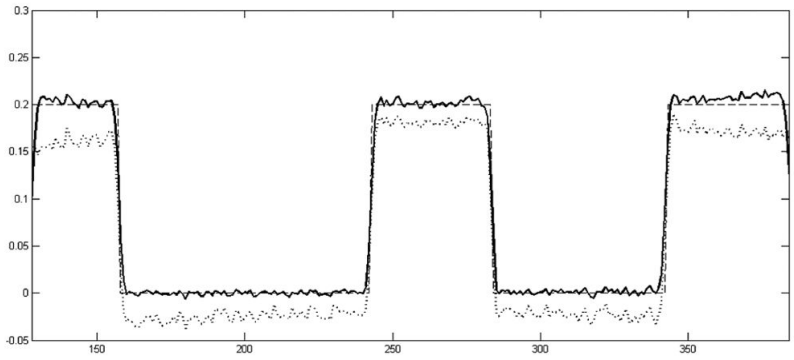

(c)

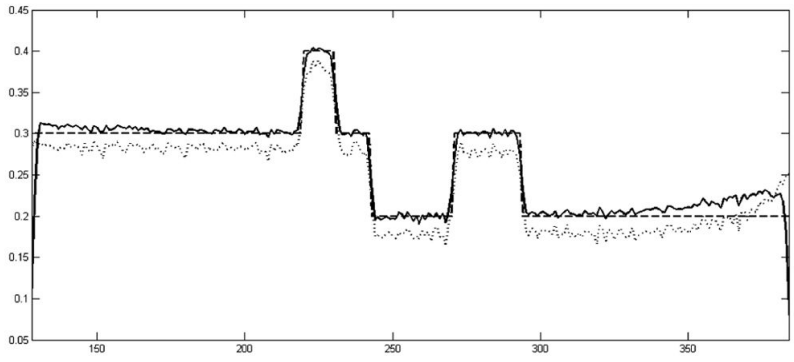

(d)

Fig. 7. (a) reconstructed image with truncated projections using FBP method with extrapolation. (b) reconstructed image with truncated projections using the iterative algorithm Eqs (56, 57, 58). (c) horizontal profiles of the reconstructed images. (d) Vertical profiles of the reconstructed images. In the profiles only the part inside the ROI is shown.

extrapolation which is defined in the following

$$E\,p_t(\theta,u)=\begin{cases}\exp(-(\frac{u+l}{\alpha L})^2)\Pi(a_-u^2+b_-u+c_-) & u<-l\\ p_t(\theta,u) & |u|\leqslant l\\ \exp(-(\frac{u-l}{\alpha L})^2)\Pi(a_+u^2+b_+u+c_+) & u>l\end{cases} \tag{63}$$

where E is the extrapolation operator. $p_t=p_t(\theta,u)$ represents the truncated projections. θ is the angle of projection and u is the position of the channel of the detector. $\pm l$ is the boundary position the detector. In this example $l=128$. L is the length of extrapolation. In this example $L=128$. $c_\pm=p_t(\theta,\pm l)$, $b_\pm=\pm\frac{\partial p_t(\theta,u)}{\partial u}|_{u=\pm l}$, $a_\pm=\frac{b_\pm(L+1)+c_\pm}{(L+1)^2}$. $\Pi(\bullet)$ is the operator setting negative values as zero. α is a parameter which is taken as $\alpha=0.65$ in this example.

Figure 7(b) shows the reconstruction from truncated projections using the iterative algorithm Eqs (56, 57 and 58). Figure 7(c) and 7(d) are the central profiles of Figs 7(a) and 7(b) in horizontal and vertical directions respectively. In Figs 7(c) and 7(d) the dashed lines show the values of the phantom. Dotted lines show the values of the reconstruction with FBP method with extrapolation. Solid lines show the values of the reconstruction with iterative algorithm Eqs (56, 57 and 58).

The iterative algorithm consists of only two reconstructions. The first extrapolation is defined in Eq. (63). The second extrapolation of the iterative algorithm E is chosen as exponential extrapolation which is defined as the following,

$$E\,p_t(\theta,u)=\begin{cases}p(\theta,-l)\,\exp(-(\frac{u+l}{\beta L})^2) & u<-l\\ p_t(\theta,u) & |u|\leqslant l\\ p(\theta,l)\,\exp(-(\frac{u-l}{\beta L})^2) & u>l\end{cases} \tag{64}$$

β is a parameter which is taken as $\beta=0.068$. Other variables are all the same as that in the extrapolation of the first reconstruction.

The truncation artifacts close to the boundary of the ROI can be seen clearly in Fig. 7(a). The truncation artifacts in Fig. 7(b) compared to Fig. 7(a) are reduced remarkably. Details of comparisons can be seen in the profiles of Figs 7(c) and 7(d). Figure 7(c) shows that the reconstructed image inside ROI using iterative algorithm (solid line) is very close to the phantom (dashed line). Figure 7(d) shows that the reconstructed image inside ROI using iterative algorithm (solid line) has only a little departure from the phantom. The little departure is caused by the massive object (i.e. the small ellipse disk) in Ω_o.

The optimal parameters α, β can be found by minimizing the truncation artifacts for a given phantom. The optimal parameters are dependent with the shape of the phantom. Hence the iterative algorithm Eqs (56, 57 and 58) is an object-dependent algorithm. This is a disadvantage. Equation (28) has no parameters relating to the object hence it is an object-independent algorithm. Section 7 tells that the iterative algorithm Eqs (56, 57 and 58) is an implementation of Eq. (28). Hence the dependency of the iterative algorithm Eqs (56, 57 and 58) to the object should not be very strong. In practice, very good truncation-reduction results have been achieved using the above parameters for a few different phantoms, for example, Shepp Logan phantom without the massive object and the slightly modified Shepp Logan phantom with a massive object riding on the border of ROI.

For this example we do not try to show the algorithm is good at convergence. Actually the algorithm diverges after second reconstruction of the iteration. See Fig. 8. In stead we try to show that the sophistical extrapolation combine with the iterative algorithm Eqs (56, 57 and 58) can improve the reconstruction quality compared to the FBP algorithm with extrapolation along.

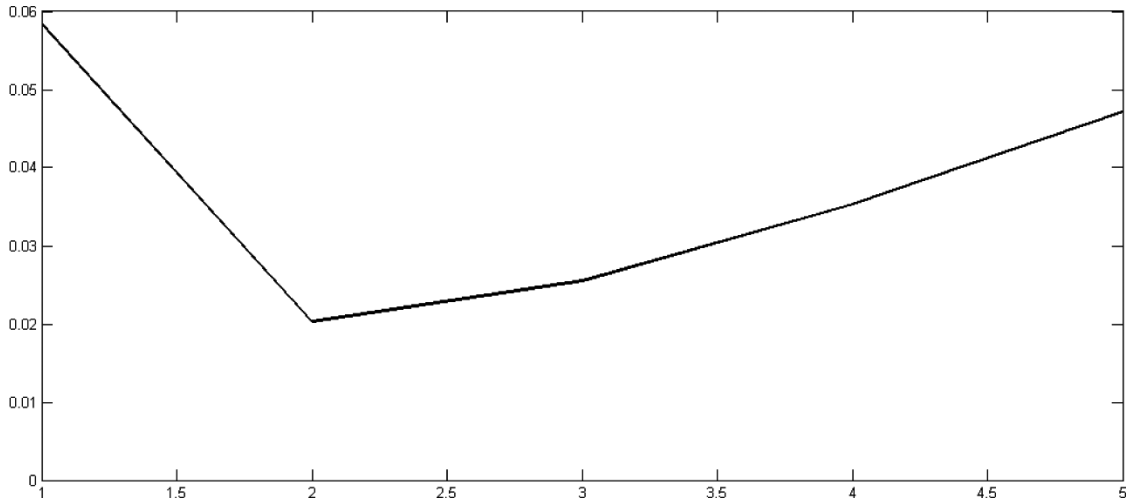

Fig. 8. The distances d corresponding to the number of reconstruction in iteration. The iterative reconstruction using strongly modified Shepp-Logan head phantom. The lowest distance is achieved in second reconstruction.

Figures 9 and 10 are the same as Figs 7 and 8 except the noises are added to the phantom. The noise are uniform distribution. The maximum value of added noises are 3% of the mean value of the projection data. With the noised data, the results are similar.

Additionally, it is known that local tomography algorithm [10,11] is more sensitive to noise than the FBP algorithm. The extrapolation algorithm is also sensitive to noise. (Especially the noise in the boundary of the FOV). The above iterative algorithm Eq. (56, 57 and 58) have more than two times of extrapolation, is it also sensitive to noise? The answer is negative. Iterative algorithm with more extrapolations is stabler than the algorithm without iteration (with only one extrapolation). It is worthy to say that the above iterative algorithm Eqs (56, 57 and 58) does not only reduce the truncation artifacts, but also reduce the normal artifacts which exists in the FBP algorithm in the case FFOV. The iterative algorithm will be further extended to FFOV in a separated publication, where the issue about noises and artifacts are discussed in detail.

9. Conclusion

In this article, CT systems are summarized as 2 assumptions. Starting from these assumptions, two algorithms for reduction of truncation artifacts are derived. In the first algorithm there are only matrix multiplications involved. The second algorithm is more sophistical because the general inverse of matrix is involved. It is proved that the error of the first algorithm is not related the object inside the ROI. Hence it is not truncation artifact free, but the interior cupping artifact is free. It is also proved that the second algorithm is a truncation-artifact-free. However the interior cupping artifact is not free. The proof utilized only the corollaries derived from the 2 assumptions. The second algorithm is similar to local tomography both are truncation artifact free. The second algorithm is referred to as local inverse in this article.

The second algorithm is implemented as an iterative algorithm. The simulation results show that the iterative algorithm with only two reconstructions can eliminate most truncation artifacts even for the phantom which has a massive object completely outside the ROI.

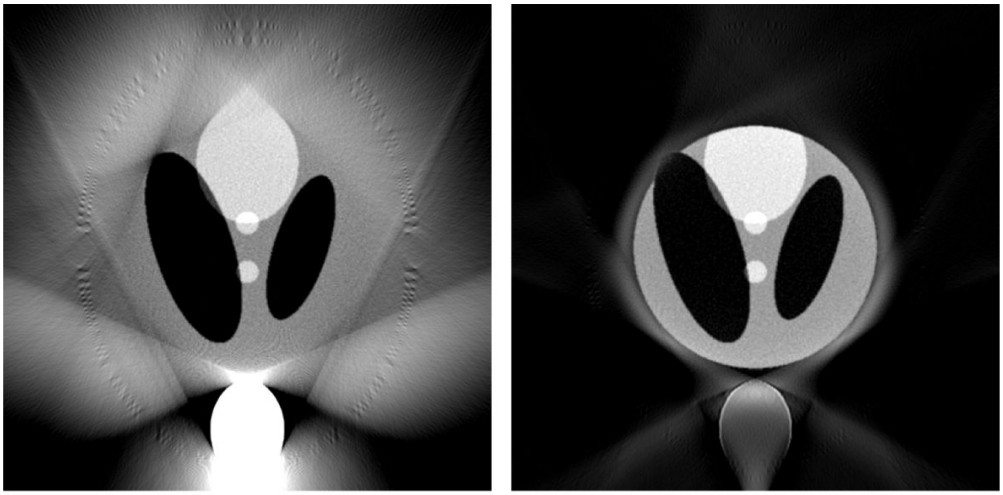

(a) (b)

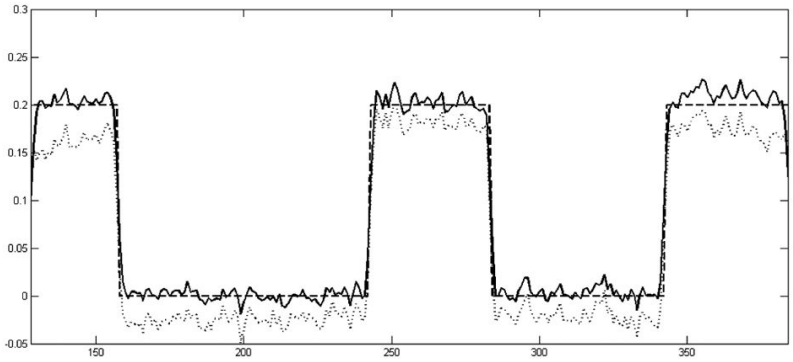

(c)

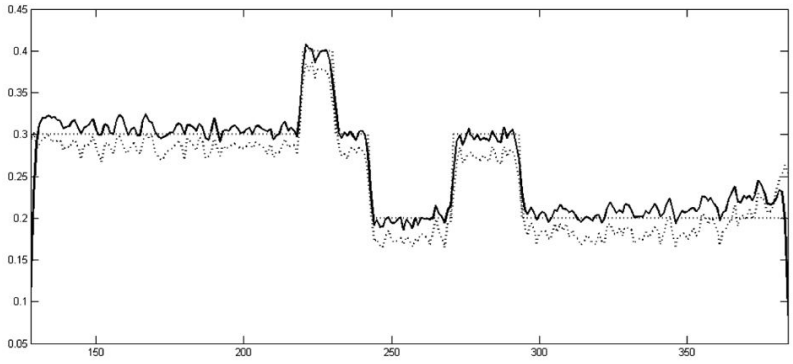

(d)

Fig. 9. (a) reconstructed image with truncated projections using FBP method with extrapolation. (b) reconstructed image with truncated projections using the iterative algorithm Eq.(56, 57, 58). (c) horizontal profiles of the reconstructed images. (d) Vertical profiles of the reconstructed images. In the profiles only the part inside the ROI is shown.

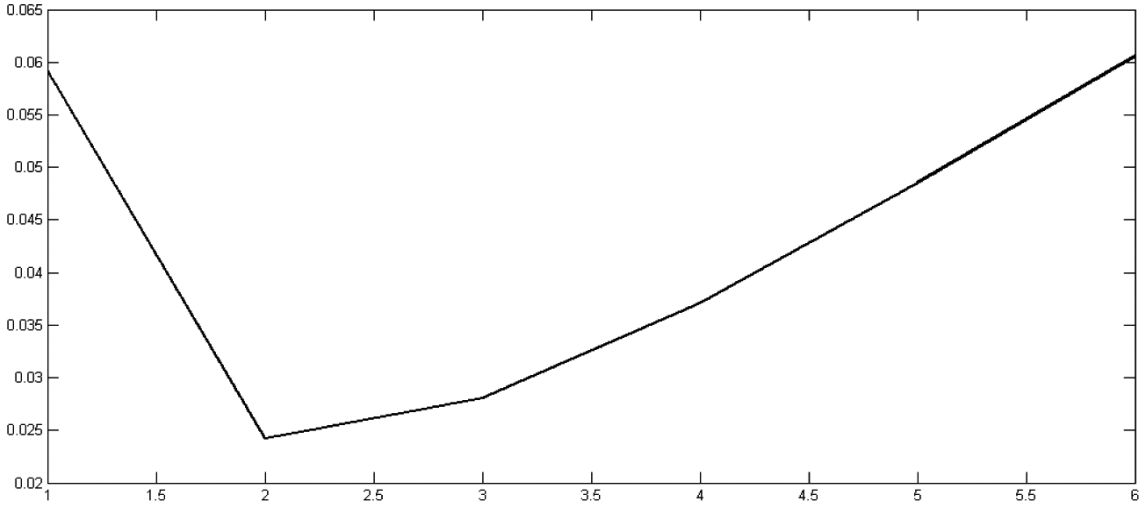

Fig. 10. The distances d corresponding to the number of reconstruction in iteration. The iterative reconstruction using strongly modified Shepp-Logan head phantom. The lowest distance is achieved in second reconstruction.

10. Future work

The future work are comparison of these two algorithms introduced in this articles with ML-EM algorithms (Maximum-Likelihood Expectation-Maximization), simultaneous algebraic reconstruction technique (SART) and local (λ) tomography. More general phantom for example suppertoroid [23] can be utilized instead of Shepp Logan Phantom. Projection data with noises should be utilized to compare the results.

General inverse of matrix should be implemented as single value decomposition (SVD) method instead of solving a linear equation using iterative algorithms.

Currently the two algorithms introduced in this article is only implemented with filtered backprojection method, it can be also implemented with Hilbert transform method [9,20]. The idea of this article using a negative inaccurate object perhaps can be utilized to reduce the error of (POCS) method [19,22].

The new applications of the concept about the local inverse in other field instead of image reconstruction should be discussed. For example if there are blurred image with very big size. If only the part of the image inside the ROI needs to be recovered from the part of blurred image on ROI, the concept of local inverse can be utilized. In this case the algorithm of local inverse perhaps can reduce the influence from outside of the ROI.

Appendix

Q^+ is generalized inverse, that satisfy that

$$Q\,Q^+Q = Q \tag{65}$$

Define matrix

$$G = I - Q\,Q^+ \tag{66}$$

There is

$$GG = G \tag{67}$$

Proof:

$$\begin{aligned} G\,G &= [I - Q\,Q^{+}][I - Q\,Q^{+}] \\ &= I - Q\,Q^{+} - Q\,Q^{+} + (Q\,Q^{+}\,Q)\,Q^{+} \\ &= I - Q\,Q^{+} - Q\,Q^{+} + Q\,Q^{+} \\ &= I - Q\,Q^{+} \\ &= G \end{aligned}$$

Further more, there is

$$G\,G\,G = G \tag{68}$$

According to the definition Eq. (65), that is

$$G^{+} = G \tag{69}$$

It can be proved that $B \perp Q$, i.e.

$$G\,Q = 0 \tag{70}$$

proof:

$$\begin{aligned} G\,Q &= [I - Q\,Q^{+}]Q \\ &= Q - Q\,Q^{+}Q \\ &= Q - Q \\ &= 0 \end{aligned}$$

References

[1] A.C. Kak and M. Slaney, 1988 Principles of computerized tomographic imaging, *IEEE Press*.

[2] B.D. Smith, Image reconstruction from cone-beam projections: Necessary and sufficient conditions and reconstruction methods, *IEEE trans Med Imaging* **MI-4**(1) (March 1985), 14–25.

[3] P. Grangeat, 1990 Mathematical framawork of cone beam 3d reconstruction via the first derivative of the Radon transform *Mathematical Methods in Tomography*, G.T. Herman, A.K Louis, F. Natterer eds., Springer Kerlag.

[4] Dan Xia, Seungryong Cho, Xiaochuan Pan, Image reconstruction in reduced circular sinusoidal cone-beam CT, Journal of X-Ray Science and Technology, 17, 189–205, 2009.

[5] M. Nilsson, 2003 Local Tomography at glance Thesis, Mathematics, Centre for Mathematical Sciences, Lund University, ISSN 1404-028X, ISBN 91-628-5741-X, LUTFMA-2007.

[6] M.M. Seger, 2002 Ramp filter implementation on truncated projection data, application to 3D linear tomography for logs Proceedings SSAB Symposium on Image Analysis, Lund, Sweden March 7–8, Editor Astrom.

[7] F. Rashid-Farrokhi, K.J.R. Liu, C.A. Berenstein and D. Walnut, Wavelet-based multiresolution local tomography, *IEEE Transactions on Image Processing* **6** (1997), 1412–1430.

[8] K.J. Ruchala, G.H. Olivera, J.M. Kapatoes, P.J. Reckwerdt and T.R. Mack, Methods for improving limited field-of-view radiotherapy reconstructions using imperfect a priori images, *Med Phys* **29** (2002), 2590–2605.
[9] F. Noo, R. Clackdoyle and J.D. Pack, A two-step Hilbert transform method for 2D image reconstruction, *Phys Med Biol* **49** (2004), 3903–3923.
[10] A. Faridani, E.L. Ritman and K.T. Smith, Local tomography, *SIAM J APPL MATH* **52** (1992), 459–484.
[11] A. Katsevich, 1999 Cone beam local tomography, *SIAM J APPL MATH* **59**, 2224–2246.
[12] M. Nassi, W.R. Brody, B.P. Medoff and A. Macovski, Iterative reconstruction-reprojection: an algorithm for limited data cardiac-computed tomography, *IEEE trans Biomed Engineering* **295** (1982), 333–340.
[13] J.H. Kim, K.Y. KWAK, S.B. Park and Z.H. Cho, Projection space iteration reconstruction-reprojection, *IEEE transaction on Medical Imaging* **4** (1983), 139–143
[14] P.S. Cho, A.D. Rudd and R.H. Johnson, Cone-beam CT from width truncated projections Computerized, Medical Imaging and Graphics **20** (1996), 49–57.
[15] S.R. Zhao and D.A. Jaffray, Iterative reconstruction-reprojection for truncated projections, *Med Phys* **31** (2004), 1719.
[16] G.H. Chen and S. Leng, 2005 A new data consistency condition for fan-beam projection data, *Medical Phys* **32**, 961–967.
[17] B. Ohnesorge, T. Flohr, K. Schwarz, J.P. Heiken and K.T. Bae, 2000 Efficient correction for CT image artifacts caused by objects extending outside the scan field of view, *Med Phys* **27**, 39–46.
[18] J. Hsieh, E. Chao, J. Thibault, B. Grekowicz, A. Horst, S. McOlash and T.J. Myers, A novel reconstruction algorithm to extend the CT scan field-of-view, *Medical Phys* **31** (2004), 2385–2391.
[19] Ye. Yangbo, Yu. 1 Hengyong 2 and GeWang, Exact Interior Reconstruction from Truncated Limited-Angle Projection Data, *International Journal of Biomedical Imaging* (2008), 1–6.
[20] Y. Zou and X. Pan, 2004, Exact image reconstruction on PI-lines from minimum data in helical cone-beam CT, *Physics in Medicine and Biology* **49**(6), 941–959.
[21] L. Zeng, B. Liu, L. Liu and C. Xiang, A new iterative reconstruction algorithm for 2D exterior fan-beam CT, *Journal of X-Ray Science and Technology* **18** (2010), 267–277.
[22] M. Defrise, F. Noo, R. Clackdoyle and H. Kudo, Truncated Hilbert transform and image reconstruction from limited tomographic data, *Inverse Problems* **22**(3) (2006), 1037–1053.
[23] Y. Hu and J. Zhu, Computed tomography simulation using supertoroids, *Journal of X-Ray Science and Technology* **18** (2010), 1–13.